RSC Advances

ROYAL SOCIETY OF CHEMISTRY

www.rsc.org/advances

<Table of Contents>

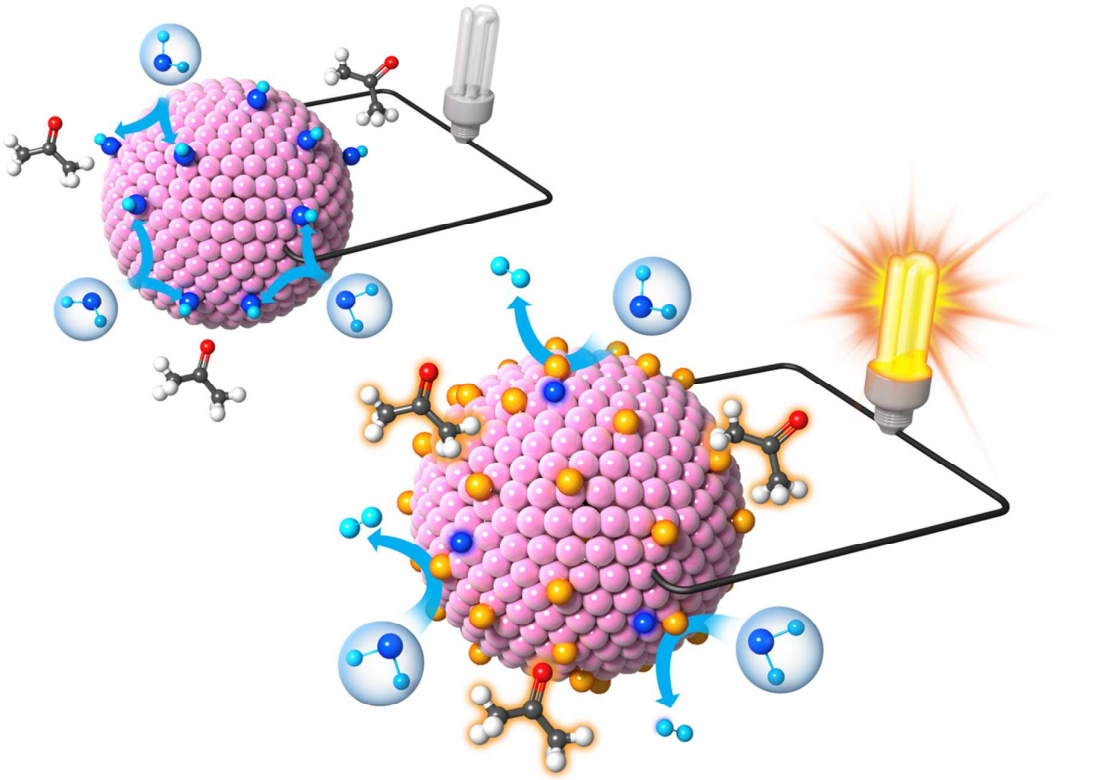

An anomalous humidity dependence of gas sensing characteristics is found on Rh-loaded WO_3 sensor where the resistance and gas response increased in humid atmospheres.

Journal Name

RSCPublishing

ARTICLE

Rh-Catalyzed WO_3 with Anomalous Humidity Dependence of Gas Sensing Characteristics

Cite this: DOI: 10.1039/x0xx00000x

Kwon-Il Choi, Su-Jin Hwang, Zhengfei Dai, Yun Chan Kang, and Jong-Heun Lee*

Received 00th January 2012,
Accepted 00th January 2012

DOI: 10.1039/x0xx00000x

www.rsc.org/

Sensing of volatile organic compounds is crucial in a variety of fields including disease diagnosis, food, and homeland security. However, significant deterioration of gas response by water vapors often hampers the sensitive and reliable gas detection in highly humid atmosphere. Herein, we report an Rh-loaded WO_3 hollow spheres chemiresistive sensor that can be potentially used for acetone gas analysis in highly humid atmosphere. The pure WO_3 and Rh-loaded WO_3 hollow spheres are synthesized based on the spray pyrolysis method. The Rh-loaded WO_3 sensor has achieved a fast acetone response (2 s), high sensitivity, good linearity, high stability, low detection limit (40 ppb) and strong selectivity to acetone even under highly humid (80% RH) atmosphere, comparing with the unloaded WO_3 sensor. Interestingly, an abnormal phenomenon happens only on n-type Rh-loaded WO_3 sensor where the resistance and gas response increased in humid atmospheres. The sensing mechanism by Rh loading is also addressed. Unusual improvement of gas response, selectivity, responding kinetics by Rh loading can probably show a good potential in acetone gas detection.

1. Introduction

Sensing of volatile organic compounds (VOCs) is crucial in a variety of fields including disease diagnosis, food, homeland security, *etc*.[1] Some of them have disease biomarking (*e.g.* acetone for diabetes), toxic, flammable or other hazardous characteristics, making the monitoring and detection of trace VOCs of prime importance.[2] Recently, metal-oxide semiconducting (MOS) materials have been indicated as good candidates for VOC gas sensors, due to their irreplaceable advantages, such as low cost, simple fabrication, miniaturized size, portability and good compatibility with Si processes.[3]

Nowadays, numerous researches have focused on the highly active nanomaterials including nanoparticles,[4] one-dimensional nanostructures,[5] nanosheets[6] and hollow spheres,[7] as well as their building blocks,[8] to develop VOC gas sensors with enhanced performances. It has been also identified that hollow and porous nanoarchitectures are more promising for large surface area to volume ratio, high gas accessibility and rapid gas responding kinetics.[9] By such porous nanostructured MOS sensors, far-ranging gases and vapors can be well detected and monitored with powerful sensitivity.[10] However, the deterioration of sensing properties by water vapors in real-atmospheres will lead to an obstacle for reliability of MOS sensors, which is an acute issue for MOS sensors. If the humidity-dependent problem could be adequately rectified, MOS hollow spheres sensors would be well suitable to serve in various application areas since they possess advantages in terms of sensitivity, rapid response and miniaturization capabilities.[7]

Gas sensing films have been doped or surface-functionalized to achieve gas selectivity.[11] Till now, numerous experimental and theoretical works were reported to detect acetone gas using modified MOS films, such as Pt-In_2O_3,[12] Pt-WO_3,[13] Cr-WO_3,[14] Si-WO_3,[15-17] graphene modified $ZnFe_2O_4$,[18] and so forth.[19] Some of them have demonstrated superior responses to acetone below 1 ppm at highly humid atmosphere (relatively humidity (RH) $\geq$ 80%) for the application of breath acetone monitoring.[16,17,20] Nevertheless, their gas sensing behaviors at varying humidity from RH 20% to RH 80% are rarely involved. In general, the introduction of water vapor in atmosphere deteriorates gas response, response/recovery speed, and selectivity to reducing gas in n-type oxide semiconductor sensors,[21] which hampers the reliable and rapid detection of trace concentration of analyte gases. Note that the enhancement of gas response in highly humid atmosphere, which is highly advantageous to detect VOC gases in real atmosphere, has been barely reported although there was a report on the enhancement of CO response by increasing humidity in Pd-loaded SnO_2 sensor.[22] Humidity-independent characteristics of gas sensor implies a possibility of exhaled breath analysis since exhaled breath contains > 80% humidity at 25 ^oC. Hence, to materialize superior sensors, it need not only pursuing a preferable sensing

material with VOCs selectivity and fast response, but also making progressive investigations on control of sensing properties in highly humid atmosphere

In this paper, we report an Rh-loaded WO_3 hollow spheres (HWs) acetone sensor that can be potentially used for real-time VOCs analysis. This sensor achieves fast response (2 s), high sensitivity, low detection limit (40 ppb) and strong selectivity to trace acetone gas even under highly humid (80% RH) atmosphere, comparing with the unloaded one. It is found that the n-type Rh-loaded WO_3 sensor exhibits an abnormal phenomenon with the resistance and gas response increased in humid atmospheres. This unusual improvement can provide a good potential in the real-time acetone gas analysis for the diabetic diagnosis application.

2. Experimental

2.1 Sample preparation

The WO_3 hollow spheres were prepared using the pre-suggested method.[23] Tungsten oxide (2.3185 g, WO_3, 99.995%, Sigma-Aldrich, USA) and Citric acid monohydrate (2.1014 g, $C_6H_8O_7$•H_2O, 99.0%, Sigma-Aldrich, USA) were dissolved in 500 mL of a 2.8–3.0% diluted ammonium hydroxide aqueous solution and stirred until the solution is clear. The solution transferred to droplet generator for the spray pyrolysis. A large amounts of droplets generated by six ultrasonic transducers (resonance freqeunce: 1.67 MHz) were carried to a high temperature (700 °C) quartz-tube reactor by a carrier gas (air, 40 L/min) and then condensed. The detailed experimental setup is shown elsewhere.[24] The condensed W-precursor were collected with a Teflon bag filter in the particle-collecting chamber and converted into WO_3 by heat treatment at 500 °C for 1 h. To load 0.5 at% Rh on the WO_3, aqueous slurry containg rhodium trichloride hydrate (0.0113 g, $RhCl_3$•xH_2O, 99.9%, Sigma-Aldrich, USA) and WO_3 (0.5 g) were stirred at 80 °C for 2 h, dried at 70 °C for 12 h, and heat treatment at 600 °C for 1 h.

2.2 Characterization

The morphologies and composition of the pure and Rh-loaded WO_3 hollow sphere were characterized using field emission scanning electron microscopy (FE-SEM, S-4700, Hitachi Co. Ltd., Japan) and transmission electron microscopy (HRTEM, JEM-ARM-200F, JEOL, USA). The phases of the samples were analyzed by X-ray diffraction (XRD, D/MAX-2500V/PC, Rigaku, Japan) and X-ray photoelectron spectroscopy (XPS, VG Multilab ESCA 2000 system, Thermo Fisher Scientific Inc., USA). To determine precise loading concentration of Rh in WO_3 hollow spheres, inductively coupled plasma spectrometer (ICP, iCAP 6300 SERIES, Thermo Fisher Scientific Inc., USA) was used.

2.3 Gas sensing characteristics

The pure or Rh-loaded WO_3 hollow spheres were dispersed in deionized water and the slurry was coated on alumina substrate (area: 1.5 x 1.5 mm^2, thickness: 0.25 mm) with two Au electrodes on its top surface (electrode widths: 1 mm, separation: 0.2 mm) and a micro-heater on its bottom surface. The sensors were dried at 70 °C for 12 h and heat-treated at 500 °C for 2 h. The sensor temperatures were controlled using the micro-heater underneath the substrate and were measured using an IR temperature sensor (Metis MP25, Sensortherm GmBH, Germany). Gas sensing characteristics were measured at 300-450 °C. The concentrations of gases and relative humidity were independently controlled by mixing between gases (100 ppm CH_3COCH_3, CO, NH_3, and 5 ppm H_2S, benzene, toluene, *p*-xylene, NO in air balance) and dry or humid synthetic air. The R_a/R_g (R_a: resistance in air, R_g: resistance in gas) values were used as the gas responses. A constant flow rate of 500 ml/min was employed and dc 2-probe resistance of the sensor was measured using multimeter (Agilent 34970A) interfaced with a computer.

3. Results and discussion

3.1 Synthesis and microstructures of Rh-loaded WO_3 HWs.

The synthesis of the WO_3 hollow spheres starts from the hollow W-precursor spheres (Figure 1a) that were prepared by ultrasonic spray pyrolysis based on our previous works.[23] After a heat treatment at 500 °C for 1 h, such precursors could be oxidized to crystalline WO_3 hollow spheres, and the morphology and sphere size are basically unchanged (Figure 1b). The corresponding transmission electron microscope (TEM) image (Figure 1c) clearly shows the hollow structures. These WO_3 hollow spheres are characterized by very thin shell thickness (~25 nm in Figure 1d), which must be beneficial to possess high gas response due to the effective electron depletion.[23] Figure 1e displays that a hollow sphere consists of highly crystalline WO_3 nanoparticles. The interplanar spacing of 3.85 Å of (001) plane and 3.69 Å of (200) with an angle of 90° reveal an orthorhombic structure. Additionally, the corresponding selected-area electron diffraction pattern (the inset of Figure 1e) demonstrates that the WO_3 HWs are polycrystalline.

With the aim to improve the exhaled breath sensing characteristics, nanoscale rhodium oxide is functionalized on the surface of the WO_3 HWs by a simple slurry mixing and after-heating. Figure 1f represents the TEM image of the Rh-loaded WO_3 HWs with a designed 0.5 at% Rh concentration ([Rh]/[W]), showing a similar morphology, size distribution and shell thickness with prototype sample (Figure 1c). The precise content of rhodium in Rh-WO_3 hollow sphere is also confirmed as 0.45 at% by inductive coupled plasma emission spectrometer (ICP) analysis. Further, elemental mapping images (Figures 1g) suggest that Rh was uniformly dispersed on the surface of WO_3 hollow spheres.

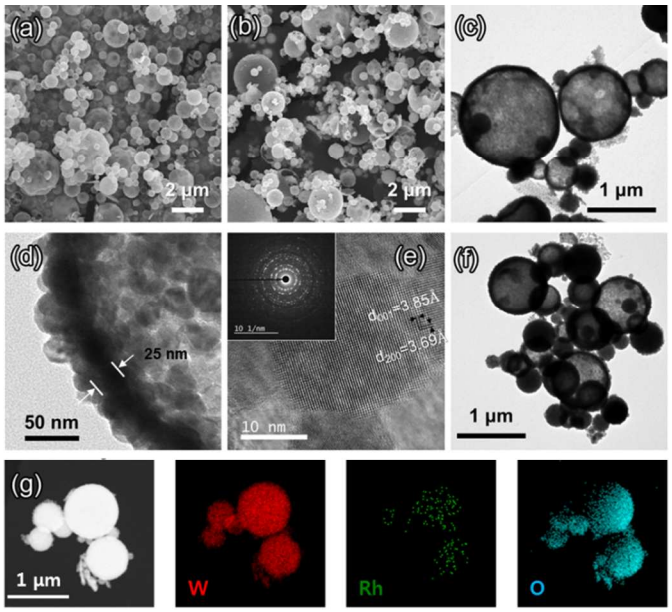

Figure 1 The morphologies and microstructures of pure and Rh-loaded WO_3 HWs. (a) SEM image of pure WO_3 HWs. (b) SEM image of Rh-loaded WO_3 HWs. (c) TEM image of pure WO_3 HWs. (d) A high-magnification view of (c). (e) The high-resolution TEM image of (d), the inset is the corresponding selected-area electron diffraction pattern. (f) TEM image of Rh-loaded WO_3 HWs. (g) elemental mapping images of Rh-loaded WO_3 HWs.

3.2 Phase and Chemical State Analysis.

Figure S1 shows the X-ray diffraction (XRD) patterns for the as-synthesized WO_3 HWs and Rh-loaded WO_3 HWs. All the peaks for both samples are well-matched with the standard WO_3 (JCPDS No.20-1324), indicating an orthorhombic structure with main growth directions (001) and (200) plane. It also shows a good consistence with the TEM results (Figure 1e). With respect to the Rh-loaded one, no Rh-related phase can be found in its XRD spectrum, owing to the small amount of Rh.

Further, the X-ray photoelectron spectroscopy (XPS) measurements were carried out to detect Rh components and determine their chemical state (Figure S2). It demonstrates that the survey scanning energy spectra (Figure S2a) for both samples are almost the same. The weak peaks located at 308.5 and 313.8 eV observed in Rh-loaded WO_3 are attributed to Rh $3d_{5/2}$ and Rh $3d_{3/2}$ in Rh^{3+} rather than metal phase Rh^0, respectively (Figure S2b).[25] The binding energies of W $4f_{7/2}$ and $4f_{5/2}$ are 35.3 and 37.4 eV (Figure S2c) in the pure sample, respectively, indicating a 6+ state of tungsten. However, binding energies of W $4f_{7/2}$ and $4f_{5/2}$ occur slight red chemical shift with 0.1 eV probably due to the increasing oxygen vacancy by Rh loading, which is similar with a previously reported Au-loaded WO_3 sample.[26] And the O 1s peak at 530.2 eV of both samples is typically ascribed to W-O in WO_3 (Figure S2d). Consequently, rhodium is stated as Rh_2O_3 rather than incorporated in the lattice of WO_3, and the increased oxygen vacancy by Rh loading may bring an enhancement of gas sensing performance by promoting oxygen adsorption.[27]

3.3 Gas sensing characteristics

Acetone gas sensing properties of pure and Rh-loaded WO_3 hollow spheres are measured in dry and various humid atmospheres. Figure 2 shows dynamic sensing transients of pure and Rh-loaded WO_3 sensors toward 10 ppm acetone gas at 400 °C in dry, 20% RH, 50% RH, and 80% RH atmospheres, respectively. In the dry atmosphere, the acetone response (R_a/R_g) of Rh-loaded sensor is ca. 13.34 (Figure 2b-1), which is about two times higher than that of the pure sensor 6.97 (Figure 2a-1). Meantime, the response and recovery time (τ_{res} and τ_{recov}, time spans taken for the response to reach [in gas] and decrease by [return to air] 90% of its steady value, respectively) is decreased from 6 s and 158 s to 2 s and 129 s by Rh loading, respectively. Hence, the sensor based on Rh-loaded WO_3 HWs exhibits enhanced acetone sensing performances than those of prototype one.

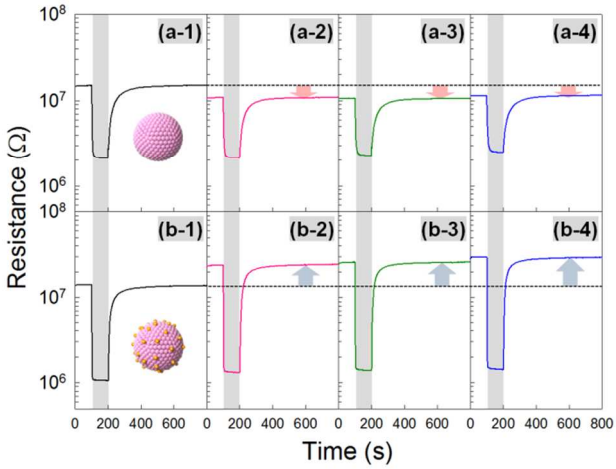

Figure 2 Transient response of pure and Rh-loaded WO_3 sensors toward 10 ppm acetone gas at 400 °C in different humidity atmospheres, respectively. (a), (b), (c) and (d) Transient responses of pure WO_3 sensors in dry ambient, 20% RH, 50% RH, and 80% RH atmospheres, respectively. (c), (d), (e) and (f) Transient responses of Rh-loaded WO_3 sensors in dry ambient, 20% RH, 50% RH, and 80% RH atmospheres, respectively.

The acetone sensing properties of the pure sensor in which R_a/R_g and R_a are decreased in wet ambient (20%~80% RH) (Figure 2a-2,a-3,a-4). This is a general behavior of n-type MOS gas sensor. For confirmation, pure SnO_2, ZnO and In_2O_3 hollow spheres were prepared by spray pyrolysis and their gas sensing characteristics were measured (Figure S3). Indeed, all the pure sensors showed the significant decreases of R_a/R_g and R_a as increasing ambient humidity, which is a normal behavior for many MOS sensors.[21] Righettoni et al.[16] also reported the deterioration of acetone sensing properties of Si-doped WO_3 in highly humid atmosphere. In stark contrast, an abnormal phenomenon happens on Rh-loaded WO_3 sensor where the R_a/R_g and R_a increased in humid atmospheres (Figure 2b-2,b-3,b-4). The sensing response at 80% RH increases from 5.70 to 20.68 after Rh loading. While the τ_{res} of pure WO_3 sensor have increased gradually from 6 s to 11 s with increasing humidity, τ_{res} of Rh-loaded sensor is keeping at 2 s throughout the humidity range. The tendency was confirmed again by continuous operation of sensor with increasing relative

humidity (Figure S4). The WO_3 HWs loaded with other noble metal catalysts (0.5 at% Pd or 0.5 at% Pt) showed significant deterioration of acetone sensing characteristics (Figure S5), confirming that the role of Rh catalyst to promote gas sensing reaction under humid atmosphere is unique and unusual.

Figure 3 presents an overview of 10 ppm acetone-sensing properties, such as R_a/R_g, R_a, τ_{res} and τ_{recov}, as functions of the working temperature and relative humidity. The R_a/R_g values of two sensors progressively increase with increasing temperature in dry and humid atmospheres (Figure 3a). And the R_a/R_g values of Rh-loaded sensor are ~2 times higher than those of pure sensor at all temperatures in the dry atmosphere. However, the two sensors have displayed different R_a/R_g *vs.* humidity tendency when varying the sensor temperature. Below 325 °C, the R_a/R_g values of both sensors decrease with increasing relative humidity. Beyond 350 °C, the Rh-loaded sensor shows an inverse behavior of R_a/R_g increasing along with the relative humidity, whereas the R_a/R_g of unloaded WO_3 sensor still decreases with the increasing humidity. Figure 3b shows the dependence of R_a on the working temperature at different humid ambient. The resistances of two sensors in dry air are similar in the whole temperature range, indicating little influence on the resistances by Rh loading. In humid atmosphere, R_a of pure WO_3 sensor decreases by water vapors whereas R_a of Rh-loaded sensor increases (marked by arrows in Figure 2) in all the temperature range (Figure 3b). In Figure 3b, we can see that the resistance of pure WO_3 sensor increases significantly by 27% when the operation temperature declining from 400 °C to 300 °C in 80% RH condition. However, the increase rate of resistance of Rh-loaded WO_3 sensor is only 3% when the temperature decreases from 400 °C to 300 °C (Figure 3b), exhibiting an anti-jamming and stable characteristic. The abnormal tendency of R_a/R_g and R_a reflect that Rh loading can probably introduce a change of humidity cross sensing mechanism at different temperatures (see the next section).

Further, we also observe the response and recovery rate of the two sensors in Figures 3 c and d, respectively. From dry to humid atmosphere, it is found that the response rate of pure WO_3 sensor becomes 1.5-2 times sluggish while τ_{res} of Rh-loaded sensor are almost invariable especially above 350 °C (see Figure 3c). It should be noted that the response speeds of Rh-loaded sensor are 2-6 and 3-12 times faster than those of pure sensor under dry and humid condition, respectively (Figure 3c). Additionally, both sensors have faster recovery speed under humid condition compared to dry atmosphere, and also the τ_{recov} of Rh-loaded sensor is shorter than that of pure one in 300 ~ 400 °C range (Figure 3d). Since all the gas sensing characteristics (R_a/R_g, τ_{res} and τ_{recov}) are significantly enhanced by Rh loading, such Rh-loaded WO_3 HWs sensor is applicable to disease diagnosis tool in effective manner.

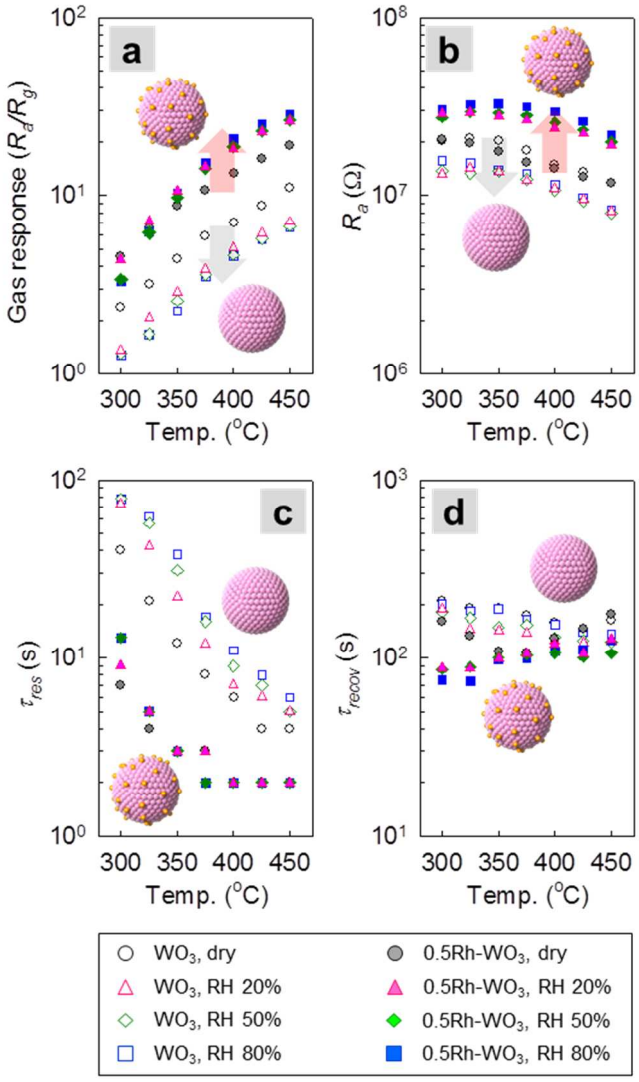

Figure 3 An overview of 10 ppm acetone-sensing properties: (a) gas response (R_a/R_g), (b) sensor resistance (R_a), (c) 90% response time (τ_{res}) and (d) 90% recovery time (τ_{recov}) as functions of the working temperature and relative humidity.

Figure 4 presents the gas response of the two sensors to 0.2~20 ppm acetone in different humidities (0-80% RH) at 400 °C, indicating a good linear relation between R_a/R_g and the gas concentration. Both sensors have stable response and recovery performances under various relative humidity conditions (Figure S6 and S7). The lowest acetone detection limit of the Rh-loaded sensor is calculated to be ca. 50 ppb and 40 ppb in dry air and 80% RH ambient when $R_a/R_g > 1.2$ was used as the criterion for gas detection, respectively, which are 4 times lower than those of the unloaded WO_3 sensor.

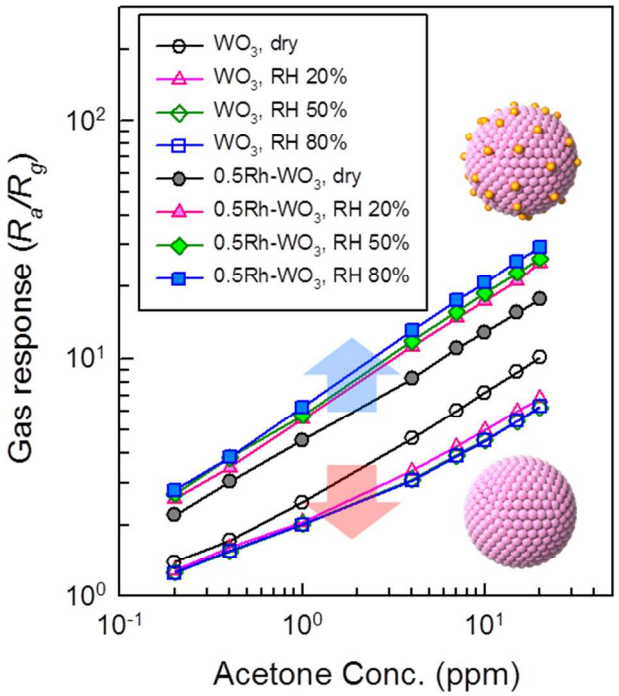

Figure 4 Gas responses of pure and Rh-loaded WO_3 sensors as functions of acetone gas concentration at 400 ºC in different humidity (0-80% RH) atmospheres.

The trace acetone detectable limit, fast response and negligible temperature-resistance dependence in highly humid atmosphere of Rh-loaded WO_3 sensor can be available for diabetes breath sensors. The key qualification for exhaled breath sensors is the selectivity of target gas, because of various interfering VOCs gases in the human exhalation, such as CH_3COCH_3 (1.8 ppm for diabetes),[28] H_2S (~ 0.5 ppm for halitosis),[29] CO (8.6 ppm for bronchiectasis),[30] NH_3 (14.7 ppm for renal failure),[31] benzene, toluene, xylene (10 ppb for lung cancer),[32] and NO (100 ppb for asthma)[33] although the precise criteria for medical diagnosis are still under investigation. Figure 5 summarizes the sensing response of the library for pure and Rh-loaded WO_3 sensors to these gases at 400 ºC in 80% RH, respectively. The concentrations of such gases are 4 ppm CH_3COCH_3, 20 ppm CO, 20 ppm NH_3, 1 ppm H_2S, 20 ppb C_6H_6 (benzene), 20 ppb toluene ($CH_3C_6H_5$), 20 ppb xylene ($(CH_3)_2C_6H_4$), and 200 ppb NO, respectively. Note that the responses toward ~2 times higher concentration of biomarker gases than the detection limit for diagnosis of diseases were measured (Table S1) to examine selectivity to CH_3COCH_3 and possible interferences from other gases more accurately. The response of pure sensor to 4 ppm CH_3COCH_3 is 3.07 (see Figure 5a), which is lower than those of 20 ppm NH_3 (Renal failure, R_a/R_g = 3.46) and 1 ppm H_2S (halitosis, R_a/R_g = 4.30). Therefore, if a patient is suffered from renal failure or halitosis, accurate diagnosis of diabetes is impossible. In contrast, the Rh-loaded sensor can overcome the above trouble of which R_a/R_g to 4 ppm CH_3COCH_3 (13.1) is 4 times higher than the protype one (see Figure 5b). This merit can makes it possible to keep a diabetes patient accurately from even a patient with either halitosis (R_a/R_g = 7.27) or renal failure patient (R_a/R_g = 3.46).

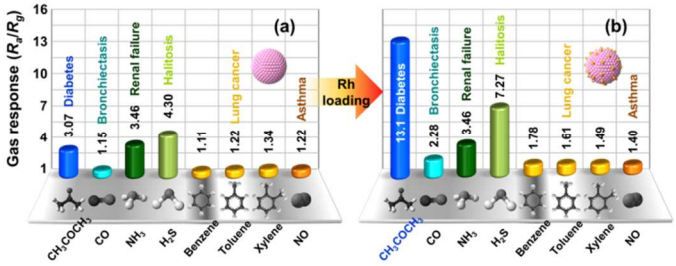

Figure 5 Bar graph summarizing gas responses of (a) pure WO_3 sensors and (b) Rh-loaded WO_3 sensors at 400 ºC to different analyte gases. Here, the concentrations of such gases are 4 ppm CH_3COCH_3, 20 ppm CO, 20 ppm NH_3, 1 ppm H_2S, 20 ppb benzene, 20 ppb toluene 20 ppb xylene, and 200 ppb NO.

3.4 Gas Sensing Mechanism.

In Figures 2a, 3a and 3b, we can observe that the R_a/R_g and R_a of pure WO_3 sensor decrease significantly in highly humid atmosphere. According the previous literature,[34] n-type semiconductor materials showing resistance decrease results from adsorbed oxygen consumption and electron generation in the presence of water vapors like as Equation (1). The R_a/R_g is also deteriorated by competition between reducing gas and water.

$$H_2O_{(g)} + O^-_{(W)} \rightarrow 2OH_{(W)} + e^- \quad (1)$$

Rh (111) has strong affinity to water compared with other metal surfaces,[35] and is easily to combine with hydroxyl group and hydrogen occurred by decomposition of water.[36] This suppresses direct reaction between sensing surface (WO_3 in the present study) and water, which prevents deterioration of gas sensing characteristics. Moreover, decomposition of water by rhodium is accelerated because co-adsorbed oxygen cut down nearly half of activation energy.[35] Therefore, more adsorbed oxygen can be formed through synergy between rhodium and surface oxygen adsorbed on metal oxide at high temperature, as depicted in Equation (2).

$$H_2O_{(Rh)} + O^-_{(W)} \rightarrow OH_{(Rh)} + OH_{(W)} + e^- \rightarrow 2H_{(Rh)} + 2O^-_{(W)} + h^+ \quad (2)$$

Since oxygen decomposed from water is adsorbed onto the sensor (WO_3) surface and ionized, depletion region on the surface of sensor will be expanded, which leads to huge change of resistance. This mechanism can well explain why Rh-loaded sensor has higher R_a/R_g and R_a in humid atmosphere. This abnormal phenomenon suggests a new direction for the real-time developing disease self-diagnosis sensor using direct analysis of highly humid exhaled breath.

If hydroxyl group does not decompose into hydrogen and oxygen sufficiently due to the energy shortage (low temperature), R_a/R_g is reduced due to the competition between target gas and water vapors reacting with surface adsorbed oxygen (O^-_W). It results to the differences of R_a/R_g changes at different sensing temperature (Figure 3a). At the low temperature like 300 °C, an decrease of R_a/R_g is induced by adsorption of hydroxyl group formed by water vapor (Equation 1). On the contrary, R_a/R_g is raised gradually due to increasing adsorbed oxygen formed by decomposition of hydroxyl group and water over 350 °C (Equation 2).

Also rhodium is known to play a role of securing selective detection of acetone gas among other VOCs,[37] which is consistent with the present results. By all accounts, the Rh-loaded WO_3 hollow spheres possesses a high response (R_a/R_g = 20.68 to 10 ppm CH_3COCH_3), rapid response time (τ_{res} = 2 s), excellent acetone selectivity and negligible temperature dependence of sensor resistance in highly humid atmosphere (RH 80%), and low detection limit (40 ppb) at 400°C which grants a rapid and reliable detection of trace acetone (Table 1).

Table 1. Gas response (R_a/R_g) to 5 ppm CH_3COCH_3, 90% response time (τ_{res}) for sensing 10 ppm CH_3COCH_3, resistance in air (Ra), and detection limit of CH_3COCH_3 of pure and Rh-loaded WO_3 sensors in dry and RH 80% atmospheres.

	Pure WO_3		Rh-loaded WO_3	
	Dry	RH 80%	Dry	RH 80%
R_a/R_g	6.97	4.57	13.34	20.68
τ_{res} (s)	6	11	2	2
R_a (MΩ)	14.91	11.43	14.06	29.53
Detection limit (ppb)	167	201	52	40

4. Conclusions

The pure WO_3 and Rh-loaded WO_3 hollow spheres were synthesized based on the spray pyrolysis method and their acetone gas sensing properties were measured in dry and various humid atmospheres (20%~80% RH). The Rh-loaded WO_3 sensor exhibited enhanced acetone sensing performances, such as fast response (ca. 2 s), four times higher response, lower detection limit (40 ppb), good linearity, high stability and strong acetone selectivity even in highly humid ambient (80% RH), comparing with the pure WO_3 sensor. Interestingly, an anomalous phenomenon happened on Rh-loaded sensor where the R_a/R_g and R_a increased in humid atmospheres, by comparing with other sensors. The abnormal sensing mechanism by Rh loading was also addressed. In addition, a low resistance (R_a)-temperature dependence of Rh-loaded sensor can grant a reliable detection of trace acetone in different external environments. This catalytic-Rh-induced unusual improvement of gas response, selectivity, responding kinetics even in highly humid atmosphere can probably show a good potential in the real-acetone gas analysis containing high concentration of water vapor.

Acknowledgements

This work was supported by the National Research Foundation of Korea (NRF) grant funded by the Korean government (MEST) (no. 2013R1A2A1A01006545).

Notes and references

Department of Materials Science and Engineering, Korea University, Seoul 136-713, Republic of Korea, Email: jongheun@korea.ac.kr; Fax: +82 2 928 3584; Tel: +82 2 3290 3282

†Electronic supplementary information (ESI) available: X-ray diffraction patterns, X-ray photoelectron spectroscopy, Gas sensing behaviors of pure and Rh-loaded WO_3 hollow spheres and other reference materials; See DOI: 10.1039/c000000x/

1 A. Modi, N. Koratkar, E. Lass, B. Q. Wei and P. M. Ajayan, *Nature*, 2003, **424**, 171-174.; T. Hoshi and S. Lahiri, *Science*, 2004, **306**, 2050-2051.; J. Kong, N. R. Franklin, C. W. Zhou, M. G. Chapline, S. Peng, K. J. Cho and H. J. Dai, *Science*, 2000, **287**, 622-625.
2 M. Phillips, K. Gleeson, J. M. B. Hughes, J. Greenberg, R. N. Cataneo, L. Baker and W. P. McVay, *Lancet*, 1999, **353**, 1930-1933.; H. Haick, Y. Y. Broza, P. Mochalski, V. Ruzsanyi and A. Amann, *Chem. Soc. Rev.*, 2014, **43**, 1423-1449.
3 Z. Dai, L. Xu, G. Duan, T. Li, H. Zhang, Y. Li, Y. Wang, Y. Wang and W. Cai, *Sci Rep*, 2013, **3**, 1669.
4 J. Qin, M. Cao, N. Li and C. Hu, *J. Mater. Chem.*, 2011, **21**, 17167-17174.
5 R. S. Devan, R. A. Patil, J. H. Lin and Y. R. Ma, *Adv. Funct. Mater.*, 2012, **22**, 3326-3370.
6 S. Some, Y. Xu, Y. Kim, Y. Yoon, H. Qin, A. Kulkarni, T. Kim and H. Lee, *Sci Rep*, 2013, **3**.
7 H.-R. Kim, K.-I. Choi, K.-M. Kim, I.-D. Kim, G. Cao and J.-H. Lee, *Chem. Commun.*, 2010, **46**, 5061-5063.; K.-M. Kim, K.-I. Choi, H.-M. Jeong, H.-J. Kim, H.-R. Kim and J.-H. Lee, *Sens. Actuators B*, 2012, **166**, 733-738.
8 K. X. Yao, X. M. Yin, T. H. Wang and H. C. Zeng, *J. Am. Chem. Soc.*, 2010, **132**, 6131-6144.
9 M. Tiemann, *Chem. –Eur. J.*, 2007, **13**, 8376-8388.; J.-H. Lee, *Sens. Actuators B*, 2009, **140**, 319-336.
10 M. A. Lim, D. H. Kim, C.-O. Park, Y. W. Lee, S. W. Han, Z. Li, R. S. Williams and I. Park, *ACS Nano*, 2011, **6**, 598-608.; X. Li, J. H. Cho, P. Kurup and Z. Gu, *Sens. Actuators B.*, 2012, **162**, 251-258.
11 M. Kimura, R. Sakai, S. Sato, T. Fukawa, T. Ikehara, R. Maeda and T. Mihara, *Adv. Funct. Mater.*, 2012, **22**, 469-476.; Z. Li, H. Zhang, W. Zheng, W. Wang, H. Huang, C. Wang, A. G. MacDiarmid and Y. Wei, *J. Am. Chem. Soc.*, 2008, **130**, 5036-5037.
12 G. Neri, A. Bonavita, Giuseppe Micali, N. Donato, *IEEE Sensors*, 2010, **10**, 131-136.
13 S.-J. Choi, I. Lee, B.-H. Jang, D.-Y. Youn, W.-H. Ryu, C. O. Park and I.-D. Kim, *Anal. Chem.*, 2013, **85**, 1792-1796.
14 L. Wang, K. Kalyanasundaram, M. Stanacevic and P. Gouma, *Sens. Lett.*, 2010, **8**, 709-712.
15 M. Righettoni, A. Tricoli and S. E. Pratsinis, *Anal. Chem.*, 2010, **82**, 3581-3587.
16 M. Righettoni, A. Tricoli, S. Gass, A. Schmid, A. Amann, and S. E. Pratsinis, *Anal. Chim. Acta*, 2012, **738**, 66-75.
17 M Righettoni and A Tricoli, *J. Breath Res.*, 2011, **5**, 037109.
18 F. Liu, X. Chu, Y. Dong, W. Zhang, W. Sun and L. Shen, *Sens. Actuators B*, 2013, **188**, 469-474.
19 S. Ryabtsev, A. Shaposhnick, A. Lukin and E. Domashevskaya, *Sens. Actuators B*, 1999, **59**, 26-29.
20 J. Shin, S.-J. Choi, I. Lee, D.-Y. Youn, C. O. Park, J.-H. Lee, H. L. Tuller and I.-D. Kim, *Adv. Funct. Mater.*, 2013, **23**, 2357-2367.
21 K.-I. Choi, M. Hübner, A. Haensch, H.-J. Kim, U. Weimar, N. Barsan and J.-H. Lee, *Sens.Actuators B.*, 2013, **183**, 401-410.; K.-I. Choi, H.-J. Kim, Y. C. Kang and J.-H. Lee, *Sens. Actuators B*, 2014, **194**, 371-376.

22 N. Barsan and U. Weimar, *J. Physics Condensed Matter*, 2003, **15**, R813.
23 Y. H. Cho, Y. C. Kang and J.-H. Lee, *Sens. Actuators B*, 2013, **176**, 971-977.
24 J.R. Sohn, Y.C. Kang and H.D. Park, Jpn. *J. Appl. Phys. 200*2, **4**1, 3006-3009.
25 A. A. Tolia, R. Smiley, W. Delgass, C. G. Takoudis and M. J. Weaver, *J. Catal.*, 1994, **150**, 56-70.
26 C. Navío, S. Vallejos, T. Stoycheva, E. Llobet, X. Correig, R. Snyders, C. Blackman, P. Umek, X. Ke, G. Van Tendeloo and C. Bittencourt, *Mater. Chem. Phys.*, 2012, **134**, 809-813.
27 N. Yamazoe and K. Shimanoe, *Sens. Actuators B*, 2008, **128**, 566-573.
28 C. Deng, J. Zhang, X. Yu, W. Zhang, X. Zhang, *J. Chromatogr. B*, 2004, **810**, 269-275.
29 F. L. Suarez, J. K. Furne, J. Springfield and M. D. Levitt, *J. Dent. Res.*, 2000, **79**, 1773-1777.
30 I. Horvath, S. Loukides, T. Wodehouse, S. Kharitonov, P. Cole and P. Barnes, *Thorax*, 1998, **53**, 867-870.
31 S. Davis, P. Spanel, D. Smith, *Kidney Int.* 1997, **52**, 223-228.
32 D. Poli, P. Carbognani, M. Corradi, M. Goldoni, O. Acampa, B. Balbi, L. Bianchi, M. Rusca and A. Mutti, *Respir. Res.*, 2005, **6**, 71.
33 S. A. Kharitonov and P. J. Barnes, *Biomarkers*, 2002, **7**, 1-32..
34 K. Grossmann, R. G. Pavelko, N. Barsan and U. Weimar, *Sens. Actuators B*, 2012, **166–167**, 787-793..
35 P. J. Feibelman, *Phys. Rev. Lett.*, 2003, **90**, 186103.
36 M. Pozzo, G. Carlini, R. Rosei and D. Alfè, *J. Chem. Phys.*, 2007, **126**, 164706.; A. Shavorskiy, T. Eralp, E. Ataman, C. Isvoranu, J. Schnadt, J. N. Andersen and G. Held, *J. Chem. Phys.*, 2009, **131**, 214707.
37 C. Houtman and M. A. Barteau, *J. Phys. Chem.*, 1991, **95**, 3755-3764.